Investigation of Underwater Hull Radiation due to Machine Noise

Xia Pan (1), Daniel Wilkes (2) and James Forrest (1)

(1) Maritime Division, Defence Science and Technology Group, Victoria, Australia
(2) Centre for Marine Science and Technology, Department of Imaging and Applied Physics, Curtin University, Perth, Australia

ABSTRACT

This paper presents the preliminary modelling and analysis of noise radiation due to the operation of machines in a compartment of an underwater vessel. The underwater vessel is modelled as a submerged cylindrical enclosure with ring stiffeners and two bulkheads. The compartment considered is between the two bulkheads. To simulate the structure-borne and airborne noise transmission and radiation, the machine noise is characterised by forces applied along the compartment in three directions and by acoustic sources located inside of the compartment. Two analytical models and three numerical models are developed. The structural and acoustic responses of the models are analysed. For a benchmark example case, the analytical and numerical results are compared with the experimental data measured in a lake.

1 INTRODUCTION

In naval applications, it is important to be able to estimate the noise radiated underwater by a vibrating hull structure due to machine noise during its design stage. Submerged cylindrical enclosures are used here as simple models to demonstrate the structural and acoustic characteristics of underwater vessels. This paper analytically and numerically investigates sound radiation from the vessel models due to machine noise.

Analytical and numerical methods are both important in the analysis of structure-borne and airborne noise. For simple structures, analytical solutions can be obtained and the mechanism of vibration and noise production can be analyzed in detail. For complex structures, numerical finite element (FE) and/or boundary element (BE) methods can be used to model vibration and noise radiation, which has made them a popular choice in recent years. However, the computing times of the numerical methods increase rapidly and instability problems may occur as the frequency increases.

Structural vibration and sound radiation from a submerged cylindrical enclosure can be modelled analytically using the following three steps. The first step is to model the free vibration of a finite hull. A critical review of the free vibration of a ring-stiffened hull was conducted by Norwood (1995). The second step is to model the excitation. The expressions for forces acting on a hull in three orthogonal directions (radial, axial and tangential) have been reported; see, for example, Pan and Hansen (1997) for a radial force and Caresta and Kessissoglou (2009) for an axial force. Recently, Pan *et al*. (2018) gave complete expressions for the radial, axial and tangential forces on a submerged cylindrical enclosure. An approximate solution for a single monopole acoustic source inside a hull was given by James (1985). This solution has been validated by Pan *et al*. (2013), where good agreement was obtained between the analytical results and results from numerical FE/BE models. The third step is to model the sound radiation from the hull. An approximation for sound radiation from a vibrating hull was given by Junger and Feit (1986), and used in Pan *et al*. (2013) and Forrest (2016).

Sound radiation from a hull submerged in water, modelled using a fully coupled FE/BE method, was reported by Peters *et al*. (2014). They applied uniform vertical, transverse and axial excitations on the hull and found that the peaks of radiated sound were primarily due to the beam bending mode of the hull. Their method was validated by Qu *et al*. (2015) using a semi-analytical method. Wilkes *et al.* (2017) applied non-negative intensity for submerged hull problems using the fast multipole BE method, which reduces computational and memory requirements and so allows solving large-scale problems at higher frequencies.

As it is difficult to measure the sound radiation in water, most published experimental results have been for a plate in air (Maidanik 1962, Fahy 1985, Oppenheimer and Dubowsky 1997). Pan *et al*. (2017) measured sound radiation of ribbed plates floating on the water surface in a water tank and compared with analytical and numerical results with good agreement. Only limited experimental results have been published on a submerged cylindrical enclosure. Burroughs and Hallander (1991) reported experimental results of sound radiation from a submerged cylindrical enclosure due to different types of force excitation. Harari and Sandman (1995) conducted similar work of sound radiation from a submerged cylindrical enclosure due to three orthogonal force excitations (radial, axial and tangential forces). They found that the importance of sound from the end plates becomes comparable with that from the cylindrical shell when the axial force was applied on the shell. However, experimental results of sound radiation from a submerged enclosure due to internal airborne noise have not been found in the literature.

The aim of the work described in this paper is to investigate analytical and numerical capabilities and limitations to estimate the underwater sound radiation due to machine noise. Two analytical and three numerical FE/BE models are developed to evaluate the sound from underwater hulls. These models are verified against each other for some cases. To validate the models, some of the modelled results are compared with the experimental data measured in a lake.

2 THEORETICAL METHOD

2.1 Simply Supported Cylindrical Shell

The first analytical model is a simply supported cylindrical shell for calculating the far-field sound pressure developed by James (1985), shown in Figure 1(a). The acoustic excitation is modelled as an internal monopole source to generate airborne noise. Figure 1(b) shows the cross-section of the shell with an interior monopole source. This model is further developed to include three orthogonal forces in this paper. Figure 1(c) shows three forces applied on the cylindrical shell in three orthogonal directions to generate structure-borne noise.

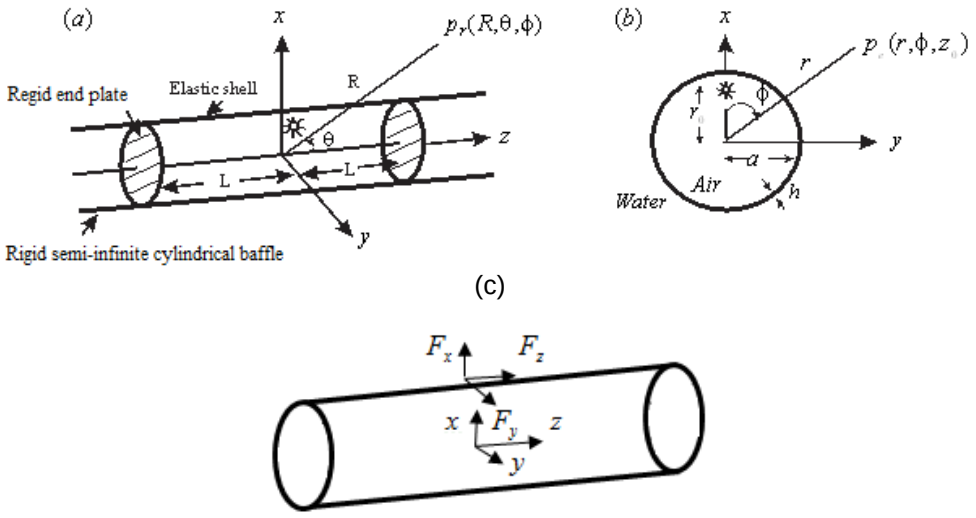

Figure 1: Geometry and coordinate systems of an analytical cylindrical shell: (a) finite cylindrical shell with rigid end plates and a monopole source; (b) cross-section of shell with a monopole source; (c) the shell with three orthogonal forces

The shell equations for this model are based on the Arnold-Warbuton formulation and modified to include water loading for a thin shell. The water loading of the shell is implemented by including the acoustic impedance of the surrounding fluid (Junger and Feit 1986). The modal amplitudes of a shell at a particular mode due to acoustic and structural excitations are obtained from the matrix relation:

$$\begin{bmatrix} S_{11} S_{12} S_{13} \\ S_{21} S_{22} S_{23} \\ S_{31} S_{32} S_{33} \end{bmatrix} \begin{bmatrix} U_{mn} \\ V_{mn} \\ W_{mn} \end{bmatrix} = \begin{bmatrix} F_{mn}^{a} \\ F_{mn}^{t} \\ F_{mn}^{r} + F_{mn} \end{bmatrix}. \quad (1)$$

The expressions of S_{ij} $(i,j = 1 \text{ to } 3)$ are shown in the reference (Pan *et al*. 2013). U_{mn}, V_{mn} and W_{mn} are the modal amplitudes in the axial, tangential and radial directions of the shell, *m* and *n* are the axial and radial mode numbers, F_{mn}^{a}, F_{mn}^{t}, and F_{mn}^{r} are the modal forces due to the axial, tangential and radial force excitation respectively, and F_{mn} are the modal forces due to the monopole excitation. These modal forces will be determined below.

As only radial displacement determines the far-field sound pressure from the shell, the radial displacement will be presented here only. The radial displacement of the submerged shell due to the radial, axial and tangential forces, and the acoustic source can be approximated by a double Fourier series as

$$W(\emptyset, z) = \sum_{m=1}^{\infty} \sum_{n=1}^{\infty} W_{mn} \sin\left[\frac{m\pi(z+L)}{2L}\right] \cdot \begin{cases} \cos(n\emptyset) & \text{for radial/axial force, source} \\ \sin(n\emptyset) & \text{for tangential force} \end{cases} \quad (2)$$

The modal forces due to the axial, tangential and radial forces can be approximated by a Fourier series as

$$\begin{bmatrix} F_{mn}^{a} \\ F_{mn}^{t} \\ F_{mn}^{r} \end{bmatrix} = \frac{e_n F_0}{2\pi a L} \sum_{s=1}^{g} \begin{Bmatrix} \cos\left[\frac{m\pi(z_s+L)}{2L}\right] \cos(n\emptyset_s) \\ \sin\left[\frac{m\pi(z_s+L)}{2L}\right] \cos(n\emptyset_s) \\ \sin\left[\frac{m\pi(z_s+L)}{2L}\right] \cos(n\emptyset_s) \end{Bmatrix} \quad (3)$$

where $e_n = 1\ (n = 0), 2\ (n > 0)$; F_0, g, z_s and $\emptyset_s$ are respectively force amplitude, number of forces and the s^{th} force location; a and L are the radius and half-length of the hull.

For a monopole source inside of a cylindrical shell, the excitation stress on the shell is given by internal pressure. The modal forces due to the monopole source are obtained from the excitation stress, given by James (1985) and developed by Pan *et al.* (2014) to include multiple sources.

The pressure radiated from a cylindrical shell to the far field due to the monopole source is given by James (1985). This pressure is extended to include three orthogonal forces as

$$p_r(R, \theta, \emptyset) = -j\omega\rho_e c_e \frac{e^{jk_e R}}{\pi R} \sum_{m=1}^{\infty} \sum_{n=1}^{\infty} \frac{G_{mn}(\alpha) e^{-\frac{jn\pi}{2}}}{\sin\theta \cdot H_n'(k_e\, a \sin\theta)} \cdot \begin{cases} \cos(n\emptyset) & \text{for radial/axial force, source} \\ \sin(n\emptyset) & \text{for tangential force} \end{cases} \quad (4)$$

where ω is the circular frequency; ρ_e, c_e and k_e are respectively the exterior fluid density, speed and wave number; $\alpha = k_e \cos\theta$ and $G_{mn}(\alpha)$ is the Fourier integral transform of the Fourier series amplitude for the cylinder's radial displacement given by James (1985).

2.2 Free Cylindrical Enclosure

The second analytical model is a free cylindrical enclosure developed by Pan *et al.* (2018) as shown in Figure 2. The shell equations for this model are based on the Flügge formulation (Flügge, 1973). Instead of a modal solution, this model uses a wave-based solution for the variation of displacements in the axial coordinate direction, while maintaining a modal sum for the circumferential direction. This model is used to present the vessel for force excitation. The expressions of displacements and far-field pressure due to three orthogonal forces are shown in the reference (Pan *et al.* 2018).

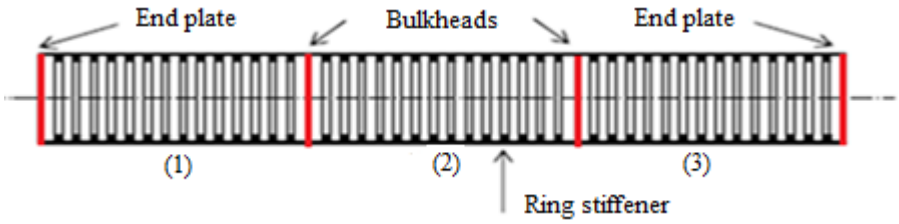

Figure 2: Cylindrical enclosure to present vessel for force excitation

3 NUMERICAL METHODS

Three numerical models were developed. The first model uses the Sysnoise method and the second model uses the fully coupled FE/BE method. These two methods are described by Pan *et al.* (2013). The third model uses the finite element method to fast multipole boundary element method (FEM-FMBEM) which will be detailed below.

3.1 FEM-FMBEM Models

The FEM-FMBEM model couples the structural FEM matrices extracted from ANSYS with a parallel broadband FMBEM model (Wilkes and Duncan, 2017) which is used to represent the exterior and/or interior fluid domains. The FMBEM reduces the computational cost of the BEM part of the model from $O(N^2)$ to $O(N\log N)$, thus allowing for large-scale models to be solved with a minimised computational cost. The FEM and BEM meshes for the discretised models consist of quadratic quadrilateral thick shell FEs and constant-unknown triangular BEs respectively, and are coupled together using a non-conforming coupling algorithm (Peters *et. al.* 2012). The FEM-FMBEM model was used to solve both the structural excitation problems due to orthogonal forces (described above), and sound radiation problems due to internal acoustic sources, as presented schematically in Figures 3 and 4 below. In the later problem configurations, the structural FEM model was coupled to both an external fluid (water) and internal fluid (air) and the acoustic fluid-structure interaction (FSI) problem solved for the structural displacements and external/internal pressures due to an acoustic point-source radiating inside one the cavities.

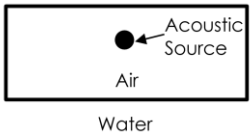

Figure 3: Short enclosure (the compartment) with acoustic source

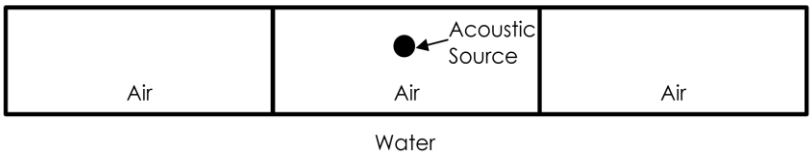

Figure 4: Cylindrical enclosure to present vessel with acoustic source

4 EXPERIMENTAL METHOD

For a benchmark example case, the experimental data obtained by Harari and Sandman (1998) for a submerged aluminium hull with length 0.79 m, radius 0.26 m and thickness 8 mm was used. The experimental cylinder with internal ring stiffeners, end plates and force location F1 are shown in Figure 5. The force F1 is radial and located on the middle stiffener. The sound pressure was measured in a lake using a hydrophone, which was located in line with the applied force and was 3.05 m above the cylinder halfway along the length. The reference (Harari and Sandman 1998) did not state how deep the cylinder was placed. We expect the cylinder would be placed well below the surface of the lake based on the similar experiment conducted by Burroughs and Hallander (1991).

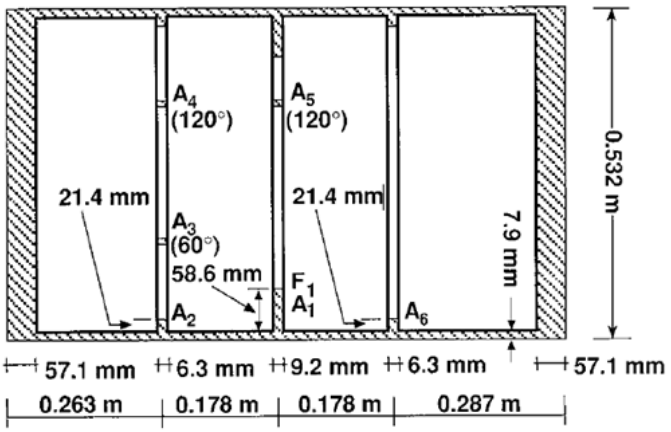

Figure 5: Experimental cylindrical enclosure with internal ring stiffeners, end plates and force location F1 (Harari and Sandman 1998)

5 RESULTS

The analytical, numerical and experimental results are shown below. The results are presented in three parts. In the first part, the sound radiation from a small compartment is presented and verification is taken against different models. In the second part, the sound radiation from a full-size vessel is presented. In the third part, the modelled results are validated against the measured data for a benchmark case. Except for Figure 9, all results are for steel structures and normalized to be per unit force or source. The far-field sound pressure was calculated at 1000 m and normalized to 1 m range by adding 60 dB. The pressure dB reference level is 1 μPa.

5.1 Sound Radiation from Small Compartment due to Airborne Noise

The first analytical model (Figure 1(a)) was compared with the published results for this model (James 1985). The comparisons are made for a submerged cylindrical enclosure with rigid end plates. The cylinder has a length 2 m, radius 1 m and thickness 10 mm. The monopole source is slightly shifted up from the origin to (r,ϕ,z) = (2a/3,0,0) in order to excite both symmetric and non-axisymmetric modes. Figures 6(a) and 6(b) show the comparisons of the far-field pressure at different elevation angles θ. The sharp peaks are the air modes in the air enclosure with rigid boundaries, while some less significant peaks correspond to the resonances of acoustically efficient shell modes (James, 1985). This statement was also proved numerically by the authors (not given here). Results shown in Figure 6 indicate excellent agreement between the current implementation of the analytical model and the original results.

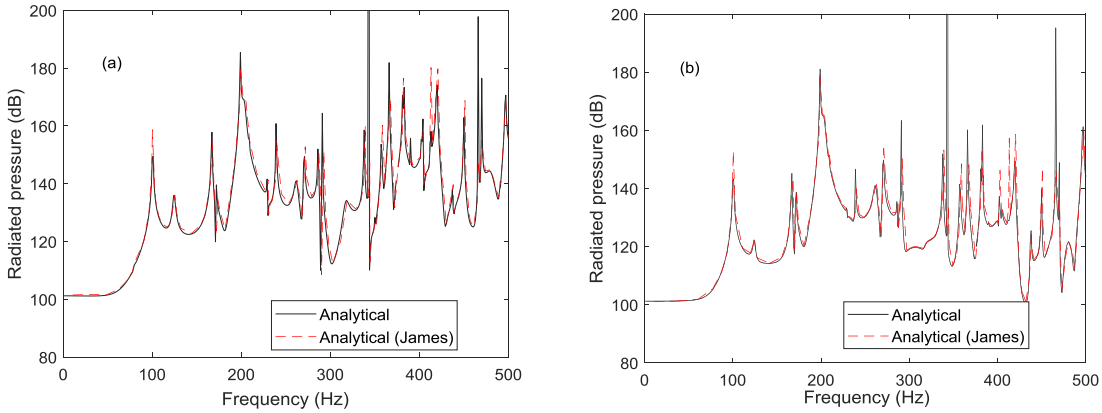

Figure 6: Sound pressure from small compartment with monopole source at (r,ϕ,z) = (2a/3,0,0) for two observation points: (a) $\theta = 90^0$ and $\emptyset = 0^0$; (b) $\theta = 30^0$ and $\emptyset = 0^0$

The analytical model was then compared with a fully coupled FE/BE model (Pan *et al.* 2013). The comparisons are made for a submerged cylinder with length 10 m, radius 1 m and shell thickness 10 mm. Figures 7(a) and 7(b) show the comparisons of the pressure from the analytical and numerical methods for two source locations.Good agreement is achieved between the two methods over the whole frequency range except for a few

points at high frequencies, which is most likely due to computational errors, slight differences between the end-plate boundary conditions, and the chosen thin shell theory. The differences between the boundary conditions and shell theory in the two models are detailed by Pan *et al.* (2013).

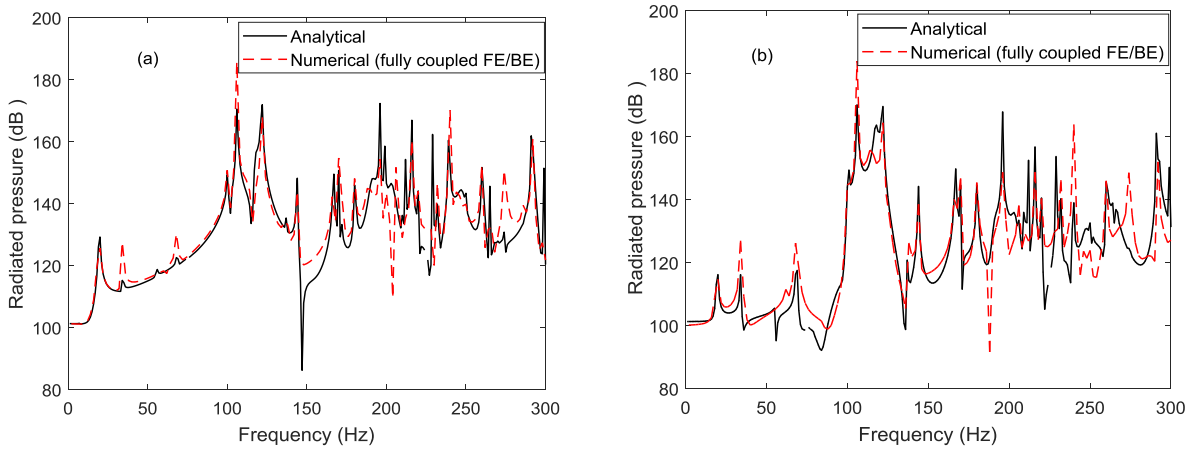

Figure 7: Sound pressure from small compartment at $\theta = 90^0$ and $\emptyset = 0^0$ for two monopole source locations: (a) $(r, \phi, z) = (2a/3, 0, 0)$; (b) $(r, \phi, z) = (2a/3, 0, 4.5)$

5.2 Sound Radiation from Vessel due to Machine Noise

In this section, the results from a vessel were calculated using the second set of analytical and numerical models (Figures 2 and 4). The machine noise was simulated by a force and an acoustic source applied to the vessel.

5.2.1 Vessel in the axisymmetric case

The Sysnoise and FEM-FMBEM methods described in Section 3 are used to verify the analytical methods. For an initial comparison, only the results for the vessel (Figure 2) without internal structure and due to an axial force applied to the centre of one end plate will be compared. The comparisons are made for a vessel with length 45 m, radius 3.25 m and thickness 40 mm. Figure 8 compares the far-field pressure obtained from the three methods. Good agreement is obtained from all the methods.

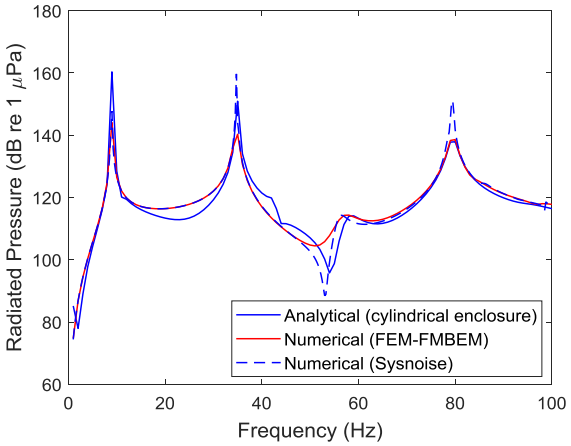

Figure 8: Sound pressure from vessel at $\theta = 90^0$ and $\emptyset = 0^0$ due to an axial force applied to the center of one end plate

5.2.2 Vessel with three orthogonal forces

This section presents the numerical results of the vessel with internal structure (ring stiffeners and bulkheads, see Figure 2) using the FEM-FMBEM method. Figure 9 presents far-field pressure due to three orthogonal forces located halfway along the vessel length. Figure 9(a) shows the pressure calculated at $\theta = 90^0$ and $\emptyset = 0^0$, which is in the same plane as the driving force. The pressure at this observation point due to the radial force is much higher than those due to the axial or tangential force. Figure 9(b) shows the pressure calculated at

$\theta = 90^0$ and $\emptyset = 90^0$. In Figure 9(b), the pressure due to the radial force and the pressure due to the tangential force are both comparable, as the observed pressure is located in the same direction as that of the tangential force.

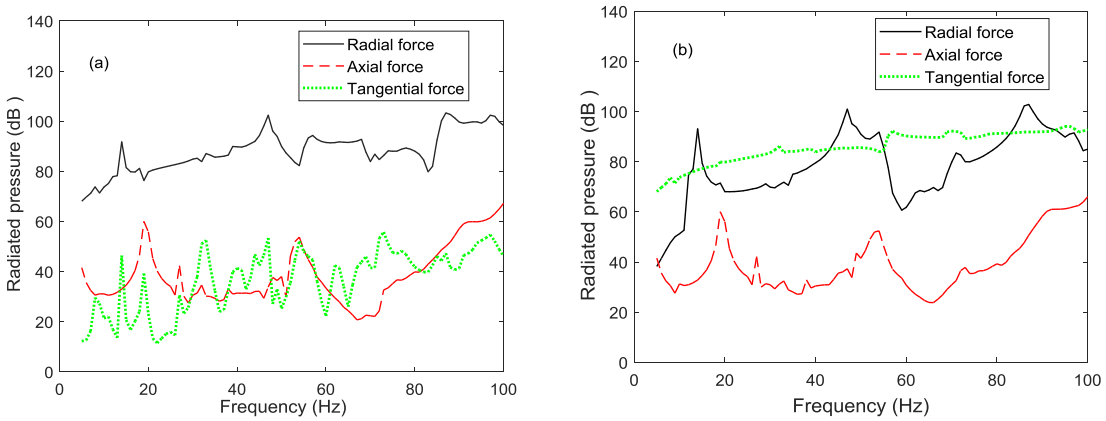

Figure 9: Sound pressure from vessel due to three orthogonal forces on the halfway of the length for two observation points: (a) $\theta = 90^0$ and $\emptyset = 0^0$; (b) $\theta = 90^0$ and $\emptyset = 90^0$

5.2.3 Vessel with airborne noise

For an initial test, the FEM-FMBEM numerical results are presented for one compartment of the vessel with flexible end plates (Figure 3). The compartment has a length 15 m, radius 3.25 m and thickness 40 mm. A monopole source is located at the centre of the interior domain. Figures 10(a) to 10(d) respectively show the interior pressure on the shell surface, exterior pressure on the shell surface, far-field sound pressure at $\theta = 90^0$ and $\emptyset = 0^0$ and total radiated sound power. Figure 10(a) shows that airborne noise inside the air enclosure propagates from the source location towards two end plates with similar pattern. Figure 10(b) shows significant airborne noise radiated from the end plates into the water. This is because the end plates are flexible so they can radiate efficiently. The peaks in Figures 10(c) and 10(d) are the air modes in the air enclosure with flexible boundaries.

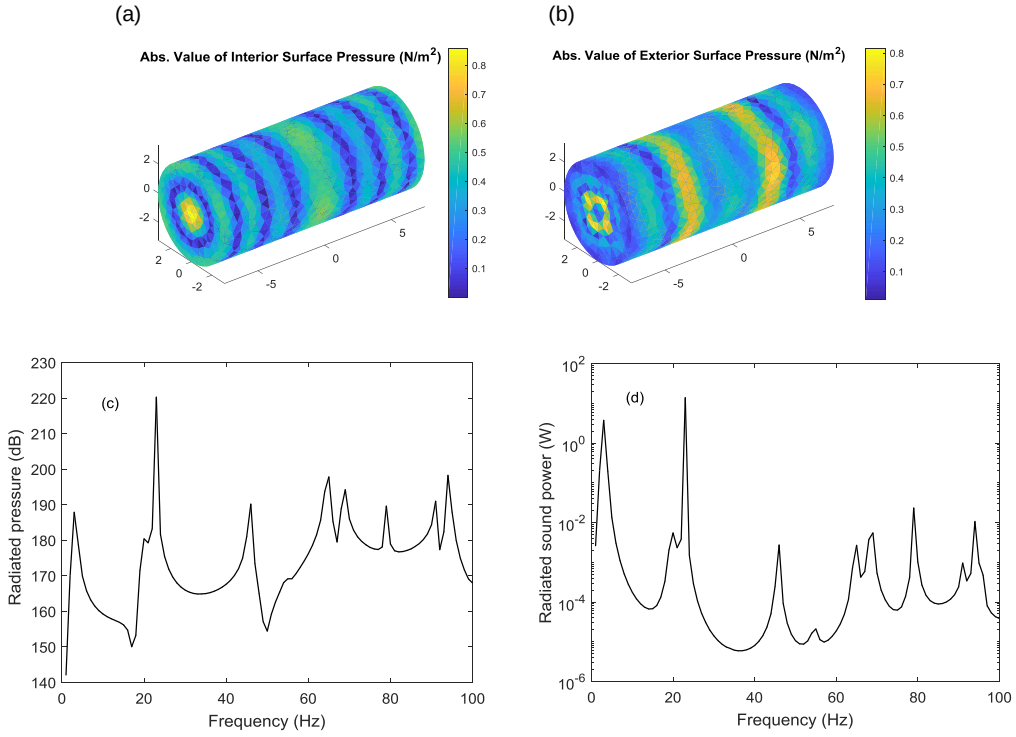

Figure 10: Compartment of vessel with monopole source at center: (a) interior pressure at 100Hz; (b) exterior pressure at 100Hz; (c) far-field sound pressure at $\theta = 90^0$ and $\emptyset = 0^0$; (c) radiated sound power

In the next case, the numerical FEM-FMBEM results are presented for a vessel (Figure 4) with length 45 m, radius 3.25 m and thickness 40 mm. A monopole source is located at the centre of the vessel, in the centre of the middle compartment. Figures 11(a) to 11(d) respectively show the interior pressure on the shell surface, exterior pressure on the shell surface, far-field sound pressure at $\theta = 90^0$ and $\emptyset = 0^0$ and total radiated sound power. Comparing Figures 11(a) and 11(b) with Figures 10(a) and 10(b) respectively, it was found that the noise from the end plates of the vessel was much lower than that from the compartment alone. This is because the noise from the end plates of the single compartment directly enters to the water. In the case of the vessel with three compartments, the noise from the bulkheads of the middle compartment transmits through the first and third compartments then into the water, which reduces sound energy. The results of the model for the compartment alone are also plotted in Figures 11(c) and 11(d) for comparison. Figures 11(c) and 11(d) respectively show the pressure and power from the vessel are lower than those from the compartment alone at low frequencies, and similar amplitudes at higher frequencies. At low frequencies, this is due to the lower end radiation as described above. At higher frequencies (wavelengths are short), the noise radiation is much more localised, and so similar noise amplitudes are obtained.

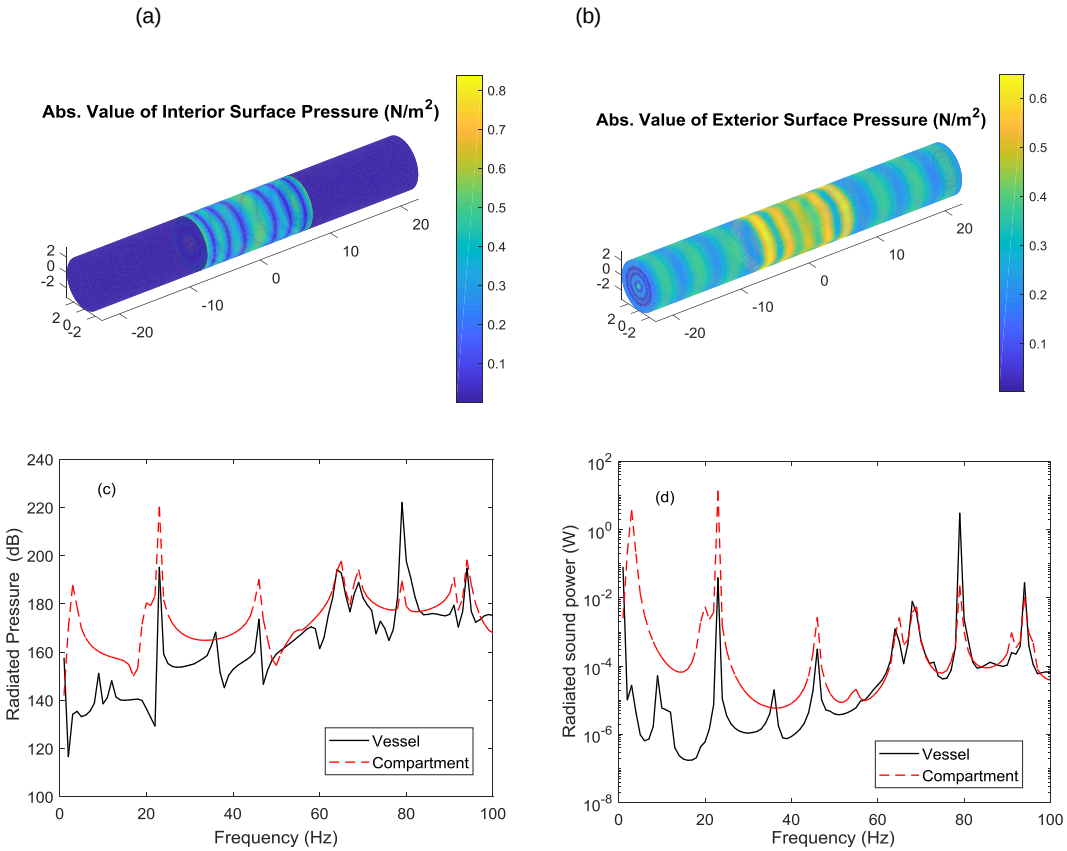

Figure 11: Vessel with monopole source at center: (a) interior pressure at 100Hz; (b) exterior pressure at 100Hz; (c) far-field sound pressure at $\theta = 90^0$ and $\emptyset = 0^0$; (d) radiated sound power

5.3 Comparison with Experimental Results

To validate the analytical and numerical models, some of the modelled results will be compared with published experimental data that was measured in a lake. The configuration of the experimental model is described in Section 4.

The results from the compartment analytical shell model (Figure 1(c)), with the same length, radius and thickness as the experimental model but without end plates and without internal structure, were compared with results from the numerical FEM-FMBEM model and the measured data. Figure 12 shows the comparison of the sound pressure from the analytical, numerical and experimental methods for a radial force excitation. Results shown in Figure 12 demonstrate reasonable agreement of the three methods but with some differences as described below.

Both analytical and numerical results predict very similar frequencies/magnitudes for the first resonance peak, while that in the experimental result occurs higher. This suggests there might be some experimental set-up which affects the experimental result. This is because the cylinder was not neutrally buoyant but held in place with cables or similar, which have not been represented in either model. The experimental set-up may restrain the cylinder in place which may cause a frequency shift. At frequencies below 200 Hz, the pressure from the analytical method is much lower than those from the other two methods. This is because the analytical model is a simply supported plain shell that does not include any end plate sound radiation, while the numerical and experimental models have thick end plates, ring stiffeners and relatively free boundary conditions. Also the analytical method only calculates the far-field pressure which omits the near-field pressure present at 3.75 m for frequencies below 200 Hz, while the numerical and experimental methods account for both the near-field and far-field pressure components. At higher frequencies, the numerical model results become progressively worse as the mesh discretization becomes coarser, relative to the acoustic/structural wavelength. The limited mesh discretisation was required to maintain the requisite length-to-thickness ratio for the thick-shell finite elements in ANSYS (in particular for the 57.1 mm thick end plates). Adoption of fully 3D finite elements in the FEM-FMBEM model would alleviate this issue.

Note that the simple analytical model can still capture approximately the amplitude and resonance frequencies of the radiated pressure from the complicated experimental structure at frequencies from 200 to 5000 Hz which almost covers the whole frequency range.

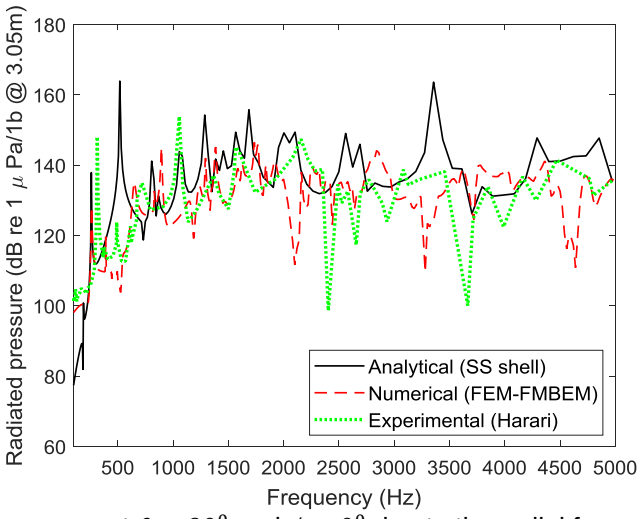

Figure 12: Sound pressure at $\theta = 90^0$ and $\emptyset = 0^0$ due to the radial force at $(\mathrm{r}, \phi, \mathrm{z}) = (\mathrm{a}, 0, 0)$

6 DISCUSSIONS AND FUTURE WORK

This paper presents a number of approaches for the modelling of sound radiation from a compartment only and a full vessel. It was found the flexible end plates of the compartment dominated the radiated sound. This therefore suggests that more realistic end boundaries are required to represent hull radiation. Hemispherical ends could be used in the future work.

It is interesting to note that the compartment analytical shell method provides reasonable agreement of sound radiation when compared with the FEM-FMBEM numerical results and experimental results. The analytical method has particular advantages over the numerical method on computational time (typically less than 30 seconds). This approach is most suitable for concept studies where a rapid assessment on a simplified initial design is required. Detailed studies for more complex structures can be conducted by a numerical approach based on the methods described in the preceding sections.

7 CONCLUSIONS

This paper has presented preliminary results and analysis of noise radiation due to representative simple sources in a compartment of an underwater vessel. Two analytical and three numerical methods have been investigated for estimating noise radiation from the compartment only and from a full underwater vessel. The vessel is modelled numerically as a submerged cylindrical enclosure with ring stiffeners and two bulkheads. It was demonstrated that noise radiated from the full model was dominated by sharp peaks associated with interior

acoustic resonances and boundaries. Also, significantly larger peaks were generated in radiated noise due to radial forcing as well as, when the direction of the forcing is in view of the observation point.

The results from the numerical vessel models were verified against those from the analytical vessel model for the axisymmetric case. Excellent agreement was obtained between the two methods. The numerical vessel model was compared with the numerical compartment model having flexible end plates for acoustic source excitation. It was found the noise from the vessel was lower than that form the compartment at low frequencies and similar at higher frequencies.

For a benchmark example case, the analytical and numerical results are compared with published experimental data measured in a lake, with reasonable agreement. This agreement indicates the feasibility of using the above methods to conduct detailed studies of complex underwater structures.

ACKNOWLEDGEMENTS
The authors would like to thank Dr Paul Dylejko, Dr Stephen Moore and Dr Ian MacGillivray for their useful discussions and suggestions.

REFERENCES
Burroughs, C.B. and Hallander, J.E. 1991. 'Acoustic radiation from fluid-loaded, ribbed cylindrical shells excited by different types of concentrated mechanical drives'. *Journal of Acoustical Society of America* 91 (5), 2721-2739.
Caresta, M. and Kessissoglou, N. 2009. 'Structural and acoustic responses of a fluid-loaded cylindrical hull with structural discontinuities'. *Applied Acoustics* **70** (2009), 954-963.
Harari, A. and Sandman, B.E.1995. *Analytical and experimental determination of the vibration and pressure radiation from a submerged, stiffened, cylindrical shell with two end plates*. Structural Acoustics, NUWC division Newport Technical Digest, 7-14.
Fahy, F.1985. *Sound and Structural Vibration: Radiation, Transmission and Response*, London: Academic Press.
Flügge, W. 1973. *Stresses in Shells*, Berlin: Springer-Verlag, 204-259.
Forrest, J.A. 2016. 'Sound radiation from a submerged stiffened cylinder with acoustic excitation'. *Proceedings of Acoustics 2016*, Brisbane, Australia.
James, J.H. 1985. *An approximation from a simply-supported cylindrical shell excited by an interior point source*. Admiralty Marine Technology Establishment, Teddington, AMTE(N) TM85024.
Junger, M.C. and Feit, D. 1986. *Sound, Structures, and Their Interaction.* An MIT Press Classic, Boston, 16-312.
Norwood, C. 1995. *The free vibration behaviour of ring stiffened cylinders - a critical review of the unclassified literature*. Report No. DSTO-TR-0200, Defence Science and Technology Organisation, Australia.
Oppenheimer, C.H. and Dubowsky, S. 1997. 'A radiation efficiency for unbaffled plates with experimental validation'. *Journal of Sound and Vibration* **199**, 473-489.
Peters, H., Marburg, S. and Kessissoglou, N. 2012. 'Structural-acoustic coupling on non-conforming meshes with quadratic shape functions'. *Int. J. Numer. Meth. Engng,* **91**, 27-38.
Pan, X. and Hansen, C.H. 1997. 'Active control of vibration transmission in a cylindrical shell'. *Journal of Sound and Vibration* **203**(3), 409-434.
Pan, X., MacGillivray, I., Tso, Y. and Peters H. 2013. 'Investigation of sound radiation from a water-loaded cylindrical enclosure due to airborne noise'. *Proceeding of Acoustics 2013*, Victor Harbor, Australia.
Pan, X., Tso, Y., Forrest, J. and Peters, H. 2014. 'Sound radiation from a water-loaded cylinder due to machine noise'. *Proceedings of Inter-noise 2014*, Melbourne, Australia.
Pan, X., MacGillivray, I., Trinh, V. and Forrest, J. 2017. 'Investigations on the total radiation efficiency of ribbed plates floating on water'. *Proceeding of Acoustics 2017*, Perth, Australia.
Pan, X., MacGillivray, I. and Forrest, J. 2018. 'Investigation of structural and acoustic responses of a submerged cylindrical enclosure under arbitrary force excitations'. *Proceedings of Acoustics 2018*, Adelaide, Australia.
Peters, H., Kinns, R. and Kessissoglou, N. 2014. 'Effects of internal mass distribution and its isolation on the acoustic characteristics of a submerged hull'. *Journal of Sound and Vibration* **333**, 1684-1697.
Qu, Y., Hua, H. and Meng, G.2015. 'Vibro-acoustic analysis of coupled spherical-cylindrical-spherical shells stiffened by ring and stringer reinforcements'. *Journal of Sound and Vibration* **355**, 345-359.
Wilkes, D.R., Peters, H., Croaker, P., Marburg, S., Duncan, A. and Kessissoglow, N. 2017. 'Non-negative

intensity for coupled fluid-structure interaction problems using the fast multipole method'. *Journal of Acoustical Society of America* **141** (6), 4278-4288.

Wilkes, D.R. and Duncan, A. 2017. 'Fast Spherical Filtering in the Broadband FMBEM using a non-equally spaced FFT'. *Proceeding of Acoustics 2017*, Perth, Australia.